JOURNAL OF MATERIALS SCIENCE 33 (1998) 1933–1939

Mechanical behaviour of a hot pressed aluminum nitride under uniaxial compression

G. SUBHASH*, G. RAVICHANDRAN
Graduate Aeronautical Laboratories, California Institute of Technology, Pasadena, CA 91125, USA

Failure strength of a hot pressed aluminum nitride (AlN) is measured as a function of strain rate under uniaxial compression. At low strain rates (10^{-6}–10^{-2} s^{-1}), the material is found to exhibit a weak strain rate sensitivity and at higher strain rates (10^{2}–10^{3} s^{-1}), a strongly strain rate sensitive behaviour is observed. The quasi-static failure strength is found to be around 2.81 GPa and it increases to 5.25 GPa at a strain rate of 2200 s^{-1}. During high strain rate testing, the specimen fractured into columnar fragments by axial splitting. Microscopic examination of the fractured surfaces revealed a typical brittle fracture with a combination of inter and intragranular failure modes. Based on the experimental results and microscopic observations, a micromechanical model has been developed to predict the constitutive behaviour of these ceramics under uniaxial compression. The model predictions of failure strength are shown to to be in agreement with the experimental observations. © *1998 Chapman & Hall*

1. Introduction

Aluminum nitride (AlN) has received considerable attention in recent years due to its wide use in many applications [1, 2]. AlN is a prime candidate as a refractory ceramic due to its high melting point (2773 K). Its excellent thermal, mechanical and corrosive resistant properties coupled with high strength makes it an ideal choice as a structural material. In spite of its potential in many structural applications, literature on its mechanical behaviour and its relation to microstructural changes is rather limited [3, 4] as compared with other structural ceramics, such as Al_2O_3, SiC and Si_3N_4. Limited bend test data at high temperatures [5], strength and fracture toughness data as a function of temperature [6] and creep data [7] are available for this ceramic. The mechanical behaviour of AlN ceramics has been investigated under confining pressure over a range of strain rates [3, 4, 8]. In these studies a brittle–ductile transition in AlN at quasi-static strain rates is demonstrated when a sufficiently high confining pressure (550 MPa) is applied. There is considerable interest in the high strain rate dependent behaviour of ceramics due to their suitability in impact applications. Lack of ample experimental data for ceramics can hinder the progress in developing constitutive models as well as design criteria.

The objectives of the present research are to investigate the uniaxial compressive behaviour of AlN at various strain rates and to obtain its failure strength as a function of strain rate. The fragments obtained from these specimens are used to characterize the deformation and failure modes using a scanning electron microscope (SEM) and to understand the mechanisms of failure and their relation to macroscopic response. In Section 2, the properties of the material and the experimental procedure adopted is briefly described. The experimental results and the microscopic observations are presented in Section 3. The relationship between uniaxial compressive strength and strain rate is discussed in Section 4. Based on the experimental results and microscopic observations, a micromechanical model is developed for the constitutive behaviour of hot-pressed ceramics. The model is described in Section 5 and the results are compared with the experimental data. Conclusions for the study are presented in Section 6.

2. Experimental procedure

2.1. Materials

The AlN used in this study (Dow Chemical Co, MI) was prepared by hot-pressing high purity powder at 1850 °C and 35 MPa for 30 min to obtain discs of 50.8 mm diameter with a theoretical density greater than 99%. The grain size was found to vary between 2 and 3 μm. The physical properties and the impurity contents of the AlN ceramic as supplied by the manufacturer are given in Tables I and II, respectively.

The effect of several additives and impurities in AlN has been investigated by several researchers. It has been found that additions of 2 wt% CaO to AlN decreases strength, hardness and toughness [9].

* *Present address*: Department of Mechanical Engineering–Engineering Mechanics, Michigan Technological University, Houghton, MI 49931, USA.

TABLE I Properties of aluminum nitride

Young's modulus, GPa	320
Bulk modulus, GPa	203
Shear modulus, GPa	129
Longitudinal wave velocity, $m\,s^{-1}$	10 700
Shear wave velocity, $m\,s^{-1}$	6300
Poisson's ratio	0.237
Flexural strength four-point, MPa	295
Fracture toughness, $MPa\,m^{1/2}$	2.8
Microhardness (Vickers 1 kg load), GPa	11.4
Thermal conductivity, $W\,m^{-1}K$	80
Thermal expansion coefficient, $1\,K^{-1}$	4.2
Heat capacity, $cal\,kg^{-1}K^{-1}$	173
Density $kg\,m^{-3}$	3250

TABLE II Impurities in aluminum nitride

O (%)	C (%)	Ca (p.p.m.)	Si (p.p.m.)	Fe (p.p.m.)
1	0.3	500	200	50

Addition of carbon inhibits the densification process and affects the thermal conductivity depending on the amount of additive. Addition of CaC_2 is found to yield uniform grain size and promote intergranular fracture.

2.2. Experimental

The hot pressed discs were cut into specimens of square cross-section with 4.06 mm sides and 7.62 mm length. Some specimens were also made into right-circular cylinders of 4.6 mm diameter and 7.62 mm length. The loading faces were kept extremely parallel (within 2.5 μm) to avoid unacceptable non-uniform strains during initial stages of loading under uniaxial compression. Axial and transverse strain gauges were mounted on the lateral surfaces of the specimens to measure axial and transverse strains during the deformation. Low strain rate experiments (10^{-6}–$10^{-2}\,s^{-1}$) were performed on a 250 kN servo-hydraulic axial–torsional materials testing system (MTS). High strain rate experiments (10^{2}–$10^{3}\,s^{-1}$) were performed using a modified split Hopkinson (Kolsky) pressure bar (SHPB) [10–15]. The loading faces were lubricated to avoid frictional effects between the specimen and the bars during loading.

Traditionally, the SHPB technique is used to investigate the plastic behaviour of metals at high strain rates. While testing very hard and brittle materials like ceramics and ceramic composites in a SHPB, suitable modifications need to be incorporated in the experimental technique as well as in the design of the specimen to obtain reliable and accurate data. These modifications have been found to be effective in determining true failure strengths and identifying failure modes under uniaxial compression. The details of the technique, the modifications required while testing hard ceramics and their necessity, as well as the limiting strain rates that can be obtained while testing ceramics using this technique have been discussed extensively in recent literature [4, 11–15].

3. Results

3.1. Mechanical response

A total of 18 tests were performed on AlN specimens at various strain rates. Five of these tests were conducted under quasi-static loading conditions in a servo-hydraulic MTS machine and the rest were conducted at high strain rates in a SHPB. The stress–strain curves for various strain rates from 10^{-5} to $10^{3}\,s^{-1}$ are shown in Fig. 1. The stress–strain curves indicate that the response is essentially linear up until failure. The initial slopes of the stress–strain curves compare well with the modulus of AlN (Table I). Also, note that the failure strain and hence the failure strength increases with increasing strain rate. The failure strength versus strain rate is plotted in Fig. 2. The failure strength remains nearly constant at 2.81 GPa at low strain rates and rises rapidly as the strain rate is increased beyond a critical strain rate. A compressive failure strength of 5.25 GPa is measured at a strain rate of $2200\,s^{-1}$. The failure strength has a rate sensitivity exponent of 0.29 at high strain rates.

All the specimens tested at low strain rates failed catastrophically, resulting in tiny fragments (powder). During high strain rate loading in a modified SHPB, the specimens failed into long columnar fragments by axial splitting in the direction parallel to the axis of loading. Such a well defined mode of failure was obtained due to controlled loading resulting from pulse shaping in the modified SHPB [4, 11–15].

3.2. Microscopic observation

Fig. 3 reveals the initial microstructure of the surface of a polished and thermochemically etched AlN specimen using the following procedure [16]. The specimen was polished with 0.25 μm diamond paste, and chemically etched in a mixture of two parts of 99.9999% phosphoric acid and one part of 99.999% nitric acid for about 3 min. Then it was thermally etched for 10 min at 1100 °C. The grain size of AlN was found to vary between 2 and 3 μm. At low strain rates, the specimens became powder after testing and hence no microstructural observations were possible. At high strain rates, columnar fragments were recovered and

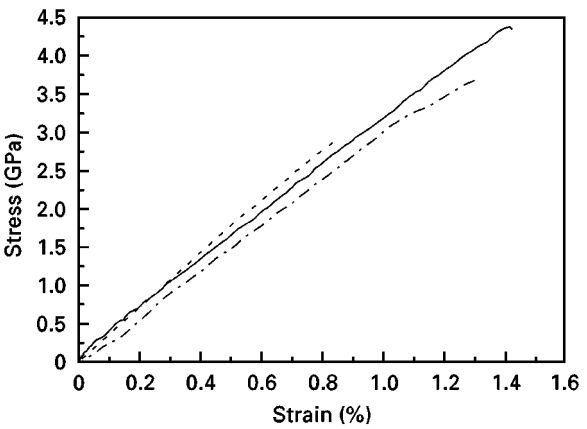

Figure 1 Stress–strain curves for hot pressed AlN at strain rates of (- - -) 2.8×10^{-5}, (- · -) 320 and (—) $900\,s^{-1}$.

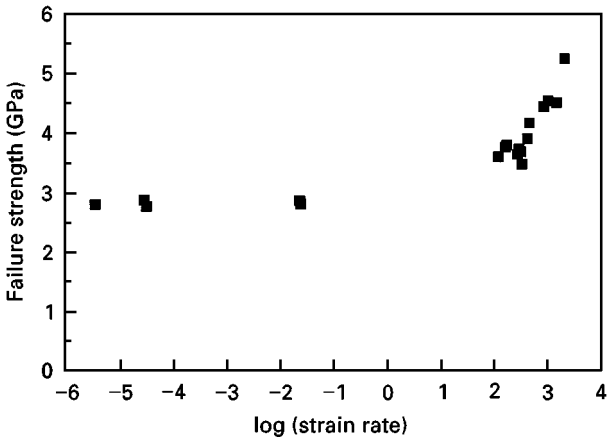

Figure 2 Plot of compressive strength versus strain rate for hot pressed AlN.

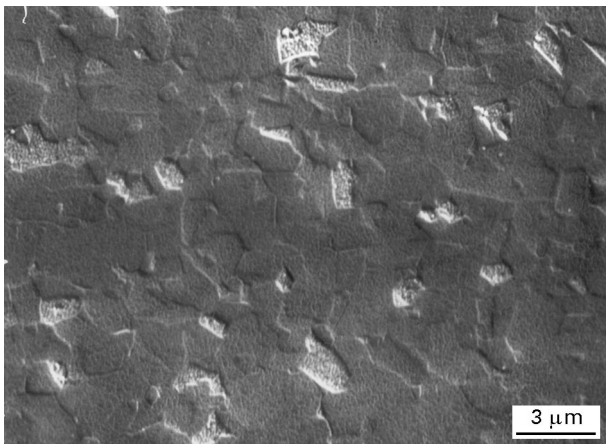

Figure 3 A scanning electron micrograph of the polished and thermochemically etched surface of undeformed AlN.

were used for microstructural observations using an SEM. The fracture surfaces contained several river-like patterns running parallel to the loading axis, as shown in Fig. 4. These river patterns are typical features of brittle fracture. This microstructure is also indicative of a combined inter and intragranular (mixed mode) fracture. It is interesting to note that the microstructure changes considerably at the two locations denoted by A and B on the micrograph. In region A, the fracture mode is predominantly intergranular as shown in Fig. 5a. In region B, there are no significant microstructural features and a transgranular fracture mode is dominant as revealed in Fig. 5b. The reason for this difference in microstructure is speculated to be a variation in the composition and contents of impurities across the specimen. It is found that doping AlN with CaO changes the fracture mode from transgranular to intergranular with concurrent decrease in hardness, strength and toughness [9]. Impurities like CaC_2 are also found to promote intergranular fracture. The variation in grain size can also significantly affect the strength and toughness values of AlN. On several other fragments, the microstructural features did not reveal any variation on the fracture surface and the fracture mode was purely transgranular, as shown in Fig. 6.

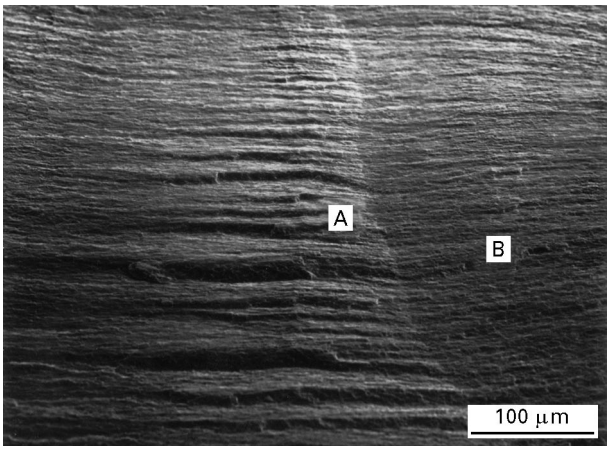

Figure 4 A scanning electron micrograph of the fracture surface of AlN revealing typical brittle fracture at high strain rates; the river markings are parallel to the direction of loading. Region A is on the ridge and Region B is outside the ridge.

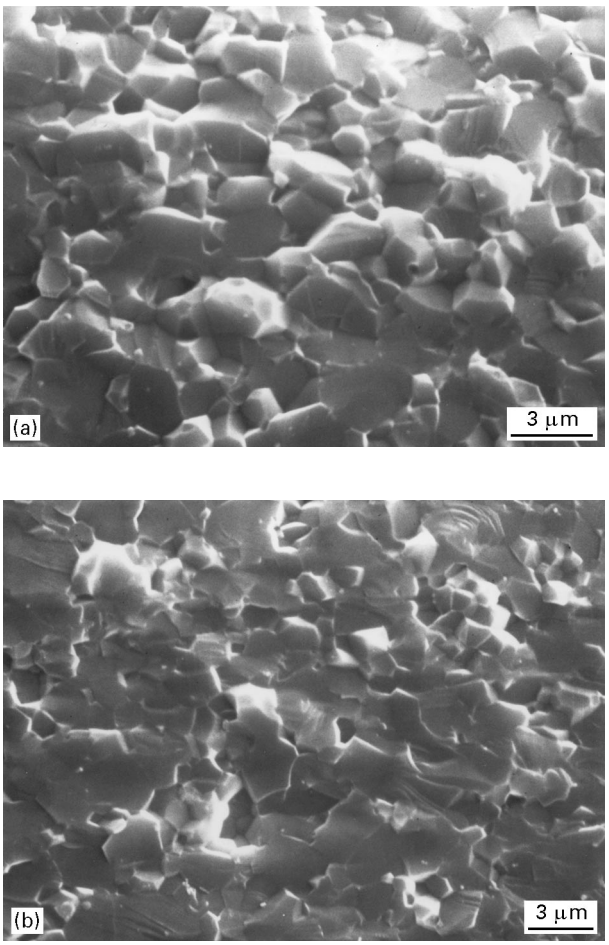

Figure 5 Scanning electron micrograph illustrating the fracture mechanisms in AlN for: (a) Region A in Fig. 4, predominantly intergranular; and (b) Region B in Fig. 4, predominantly transgranular.

4. Discussion

It is clear from the plot of Fig. 2 that hot pressed AlN is weakly rate sensitive at low strain rates and strongly rate sensitive beyond a critical strain rate. It has been reported that hot pressed AlN continues to strengthen even above the Hugoniot elastic limit (HEL). The

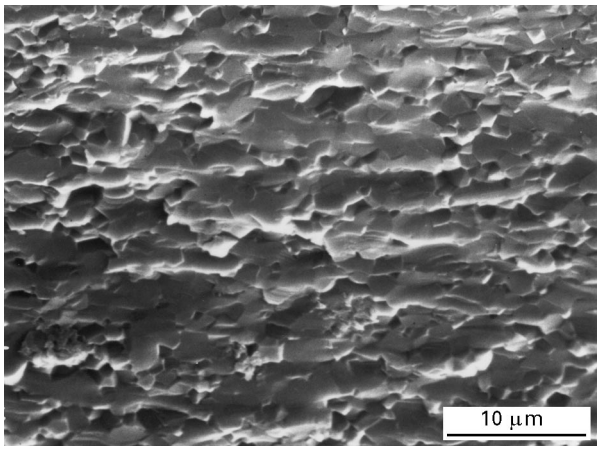

Figure 6 A scanning electron micrograph of the commonly observed transgranular fracture in AlN.

apparent increase in compressive strength beyond the HEL is attributed to either strain rate effects or to high confining pressures that exist in the shocked specimen [8].

The strain rate dependent behaviour of the failure strength of ceramics has been discussed by Lankford [17, 18]. At low strain rates, for both hot pressed and sintered ceramics, crack initiation from the pre-existing flaws is considered to be athermal, and the crack growth process is assumed to be activated thermally and is a function of the properties of the material. In the case of hot pressed ceramics, the prevailing high pressures and lack of sintering additives during processing result in good bonding between the grains, which leads to fewer in number and smaller size flaws. Under the applied compressive loads, these flaws act as sliding cracks and initiate tensile cracks that grow in a stable manner resulting in a weakly strain rate dependent behaviour. Sub-critical crack growth is also cited [19] as the reason for the observed rate sensitivity of tensile failure in the quasi-static regime.

This high rate sensitivity of failure strength is commonly observed for hot pressed as well as sintered ceramics [17]. Grady and Lipkin have modelled the process of dynamic failure and have predicted the strain rate sensitivity exponent to be one-third for failure strength of brittle materials and it is said to be independent of the properties of the material [20]. The crack initiation process is assumed to be athermal, but crack growth from the pre-existing flaws is considered to be dominated by inertial effects. Unlike in sintered ceramics, the prevailing high pressures during processing yield a lower number of uniformly distributed microcracks in hot pressed ceramics. Upon loading, tensile cracks initiate and start to grow in a stable manner once the critical stress intensity factor is reached. The dynamic crack growth is considered to be responsible for observed high strain rate sensitivity of failure strength in ceramics [17].

From an experimental point of view, the situation in hot pressed AlN follows closely the above discussion. When the specimens are tested at low strain rates in an MTS machine, all the specimens fail into tiny fragments (powder). In the absence of any toughening mechanism in a brittle ceramic, once the cracks initiate, they grow in an unstable manner and coalesce causing catastrophic failure in the specimen. Besides, the large elastic energy stored in the grips of the MTS machine continues to supply the energy for several growing cracks resulting in crushing of the specimen before the loading grips can be withdrawn.

Under high strain rate loading in the SHPB, the duration of the stress pulse is generally of the order of 100 μs and the specimen is subjected to only a single loading pulse [4, 11, 12]. When using a ramp loading pulse the duration of peak load (when the microcracking initiates) is much shorter and hence the cracks that initiate may not have sufficient time and energy to propagate and coalesce to cause complete failure of the specimen. In addition, the magnitude of the incident pulse is also predetermined in such a way that it is just sufficient to cause failure of the specimen. Because the total input energy is controlled, the specimen fractures into columnar fragments due to the growth of a fewer number of axial microcracks. During uniaxial compression it has been established that the microcracks initiate and grow parallel to the loading axis, which is typical of compression induced fracture in brittle materials [21, 22].

5. Micromechanical model

The experimental results shown in Figs 1 and 2 clearly reveal the rate sensitive nature of the failure strength of hot pressed AlN. Based on these observations, a micromechanical model is developed to predict the constitutive behaviour of ceramics under uniaxial compression. Because failure in brittle ceramics occurs by microcrack initiation, growth and coalescence, we describe the crack growth rate by two separate models in two strain rate regimes. Under quasi-static deformation the crack growth velocity is described by a power law [19] and under high strain rate deformation by the constant energy release rate criterion in dynamic fracture [23]. The failure of the material is linked to a critical density of damage or critical length for coalescing microcracks. Only a brief discussion of the model is presented here and the complete details can be found elsewhere [24].

5.1. Overview of the model

The initial distribution of microcracks is assumed to be dilutely distributed (non-interacting) and randomly oriented, as shown schematically in Fig. 7a. This enables the construction of the unit cell model shown in Fig. 7b; each microcrack is of average length $2a$ and is oriented at an angle, θ, and is assumed to be subjected to uniform uniaxial stress loading. Under uniaxial compressive stress loading conditions, the microcracks resist sliding due to the resolved shear stress on the crack faces. As the axial stress increases, the critical condition for tensile crack growth is reached at the tips of the sliding crack. The tensile cracks that emerge from the tips of these pre-existing cracks initially grow in a curved manner, and for $l > a$, grow parallel to the compression axis, where l is the current length of growing tensile cracks; see Fig. 7b. For

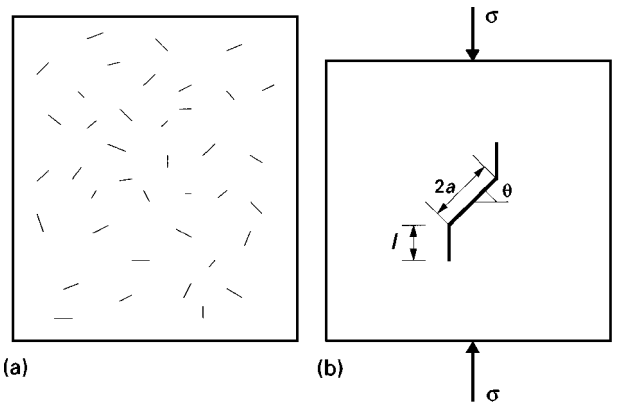

Figure 7 Schematic of (a) randomly oriented initial flaws in the specimen, and (b) a unit cell model for a sliding crack subjected to far-field uniaxial compressive loading.

simplicity, we replace these curved wing cracks by straight cracks [22]. Under compressive loading, the mode-I and mode-II stress intensity factors at the tip of the growing crack can be written as

$$K_{\mathrm{I}} = \frac{2a\tau^* \cos\theta}{\sqrt{\pi(l + l_*)}}, \qquad K_{\mathrm{II}} = \frac{2a\tau^* \sin\theta}{[\pi(l + l_*)]^{1/2}} \tag{1a, b}$$

where τ^* is the shear stress on the pre-existing microcrack that causes sliding of the two crack faces

$$\tau^* = \frac{\sigma \sin 2\theta}{2} - \tau_{\mathrm{f}}. \tag{2}$$

The frictional shear stress, τ_{f}, that resists sliding of the crack faces is given by

$$\tau_{\mathrm{f}} = \frac{\eta\sigma(1 + \cos 2\theta)}{2} \tag{3}$$

where η is the coefficient of friction. When the length of the tension cracks is small, i.e. $l = l_*$, the stress intensity factors are accurately given by Equation 1a, b [21]. l_* has been estimated to be $0.27\,c$.

The virtual energy release rate for the growing tensile crack is given by [24]

$$G(l) = \frac{1}{E}\left[\frac{4a^2(\tau^*)^2}{\pi(l + l_*)}\right] \tag{4}$$

where E is the Young's modulus of the undeformed material.

Defining the initial number of microcracks of length, a, per unit area by N, the areal density of microcracks, f_0, is given by

$$f_0 = Na^2 \tag{5}$$

Using a global energy balance approach, the relation between stress and strain under uniaxial stress conditions as $\sigma = \bar{E}\varepsilon$, where $\bar{E}$ is the effective axial modulus of a microcracking solid under uniaxial compression [24]

$$\frac{\bar{E}}{E} \approx \left[1 + p_1 f_0 \ln\left(\frac{l}{l_*} + 1\right) + p_2 f_0\right]^{-1} \tag{6}$$

The term with coefficient p_1 corresponds to the change in the modulus of the microcracked body due to axial crack growth and the term with p_2 corresponds to the change in the modulus due to sliding of the microcracks. It is important to mention that under uniaxial compressive loading, the modulus in the direction of loading does not change appreciably due to the growth of axial cracks in a brittle ceramic and for most engineering ceramics $\bar{E} \approx E$ [12, 24].

In linear elastic fracture mechanics, for brittle materials, crack growth is said to occur when the stress intensity reaches its critical value, i.e. $K_{\mathrm{I}} = K_{\mathrm{Ic}}$. Evans [19] has observed a power law relationship between the crack growth velocity, v, and stress intensity factor, K_{I}, under quasi-static loading conditions

$$v = \mathrm{A}K_{\mathrm{I}}^n \tag{7}$$

where A is a material constant and n is an exponent that is around 50–100 for ceramics. At higher strain rates, when the crack growth velocities are comparable to Rayleigh wave speeds, c_{R}, there are several criteria available in the literature [23, 25]. In dynamic fracture mechanics, the relation between energy release rate and crack growth velocity, v, can be written as a universal relation [23]

$$\frac{G_{\mathrm{c}}}{G_{\mathrm{d}}(l, t)} = \left(1 - \frac{v}{v_{\mathrm{m}}}\right) \tag{8}$$

where v_{m} is the maximum terminal velocity of the crack, G_{c} is the critical energy release rate and $G_{\mathrm{d}}(l, t)$ (Equation 4) is the virtual energy release rate for the stationary crack of current length, l. For $v_{\mathrm{m}} = c_{\mathrm{R}}$ the above expression reduces to constant energy release rate criterion [23]. In general, maximum crack speeds of 0.3–$0.5c_{\mathrm{R}}$ are observed in materials.

Further, it is reasonable to assume that the material looses its load carrying capacity when the damage reaches a critical value, f_{c}, which can be expressed as

$$f_{\mathrm{c}} = Nl_{\mathrm{c}}^2 \tag{9}$$

where l_{c} is a critical length of the tension crack when coalescence occurs with other growing cracks.

5.2. Constitutive modelling

Assuming a constant strain rate deformation, i.e. $\bar{\varepsilon} = \dot{\varepsilon}_0 t$ one can write the strain and stress relation for uniaxial stress as

$$\sigma = \bar{E}\dot{\varepsilon}_0 t \tag{10}$$

where $\bar{E}$ is the reduced modulus given in Equation 6.

The critical stress intensity factor, K_{Ic}, for crack initiation is assumed to reach when the applied compressive stress attains the value of the quasi-static compressive strength, σ_{o} i.e.,

$$K_{\mathrm{Ic}} = \frac{4a\bar{E}\dot{\varepsilon}_0 t_0}{3(\pi - 2\theta_{\mathrm{s}})}\left(\frac{1}{\pi l_*}\right)^{1/2} \times [\cos^3\theta_{\mathrm{s}} - \eta(2 - 3\sin\theta_{\mathrm{s}} + \sin^3\theta_{\mathrm{s}})] \tag{11}$$

where t_0 is the time taken for the stress to reach σ_o, which can be determined from Equation 10; θ_s is the orientation of the pre-existing microcrack for which sliding can occur, $\theta_s = \tan^{-1}(\eta)$.

Now using the fracture criteria, Equations 7 and 8 discussed before one can study the effect of strain rate on the failure strength of ceramics. For quasi-static loading, using the power law, Equation 7 along with Equations 10 and 11, one can obtain a differential equation for $v(dl/dt)$ which can be integrated using the Runge – Kutta method. Then we apply the failure criterion in Equation 9 and obtain the relation between critical crack length and critical stress intensity factor as

$$\frac{l_c}{AK_{Ic}^n t_0} = F_s\left(\frac{t_c}{t_0} n\right) \quad (12)$$

Similarly for high strain rate deformation, using Equations 8–10, we can write

$$\frac{l_c}{v_m t_0} = F_d\left(\frac{t_c}{t_0}\right) \quad (13)$$

If the relation between crack growth velocity and fracture toughness (K_I versus v) is known, the left-hand side of the above equation is known and hence F_s and F_d can be plotted as function of t_c/t_0. Knowing the failure time, t_c, and the corresponding t_0, one can predict the failure strength, $\sigma_c = \bar{E}\dot{\varepsilon}_0 t_c$, of the material for different strain rates.

A critical strain rate, $\dot{\varepsilon}_*$, at which the transition from stable crack growth under quasi-static loading rates to inertia dominated crack growth under high strain rates, can be defined in terms of material properties as

$$\dot{\varepsilon}_* = \frac{\sigma_0}{E}\frac{c_*}{l_s} \quad (14)$$

where c_* is a characteristic speed when the inertia effects become significant (usually 0.2 times the shear wave velocity, c_s) and l_s is a characteristic length (e.g. specimen length). For most engineering ceramics E/σ_o is between 100–150 and c_* is between 1200–1400 m s^{-1}.

For hot pressed AlN used in our experiments, the specimen length, l_s, is 7.62 mm, the quasi-static strength, σ_o, is found to be around 2.81 GPa, and the transitional strain rate, $\dot{\varepsilon}_*$, is calculated to be 1450 s^{-1}. A fracture toughness value, K_{Ic}, of 2.8 MPa m$^{1/2}$ is used for hot pressed AlN (Table I), and the friction coefficient, η, is assumed to be 0.6. The initial flaw size is assumed to be 3 μm, and is reasonable for AlN whose grain size varies from 2 to 3 μm. The initial areal density of defects, f_o, is assumed to be 10^{-3} which is typical for hot pressed ceramics. Assuming $l_c/v_m = 2$ μs, one can obtain the normalized compressive strength as a function of strain rate. From the available experimental evidence on the running cracks for ceramics, the maximum terminal velocity for dynamically propagating cracks, v_m, is assumed to be one-third of the shear wave velocity [26]. Because t_0 is known from the experiments at various strain rates, t_c can be computed at each strain rate using Equation 12 or 13 and hence the compressive strength, σ_c, as a function of strain rate, $\dot{\varepsilon}$. The predicted values for the failure strength are plotted along with the experimentally obtained data as a function of strain rate in Fig. 8. The predictions from the micromechanical model appear to capture the high rate sensitivity of failure strength at high strain rates. The strain rate dependence of failure strength given in Fig. 8 yields the relationship, $\sigma_c \propto \dot{\varepsilon}^m$, where $m = 0.287$. Grady and colleagues predicted $m = 1/3$ for all brittle materials based on global energy considerations relating to failure. The details of the dependence of m on other material parameters can be found elsewhere [24].

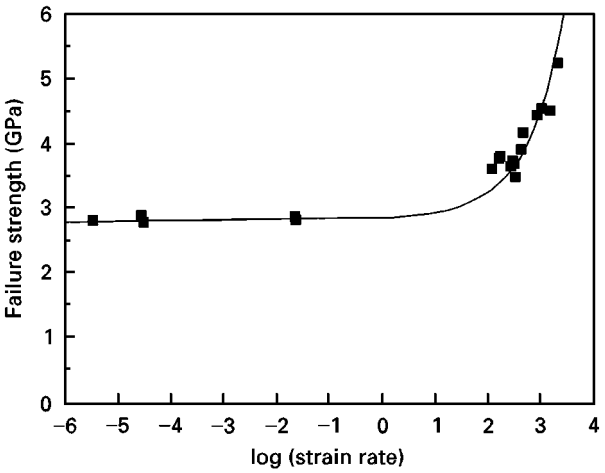

Figure 8 Comparison of predicted (—) and experimentally (□) measured uniaxial compressive strength as a function of strain rate for hot pressed AlN.

6. Conclusions

The dependence of uniaxial compressive failure strength of hot pressed AlN on strain rate is examined. At low strain rates the failure strength is found to be weakly rate dependent and at high strain rates, it is strongly rate sensitive. Microscopically the material exhibits predominantly a mixture of transgranular and intergranular fracture. This is attributed to impurities like CaO and CaC_2 present in the material. A micromechanical model applicable to both quasi-static and impact loading conditions based on sliding crack nucleation and growth is developed to predict the strain rate dependence of failure strength in these ceramics. For hot pressed AlN, the constant energy release rate criterion appears to be the most suitable one for dynamic crack propagation criterion. The model predictions of failure strength compare well with the experimental results. The results of the experiments and the micromechanical model presented here can be used to understand the complex behaviour of AlN under impact loading conditions.

Acknowledgements

The support provided by the National Science Foundation (Grant No. CMS-9157846) through a Presidential Young Investigator award to G. Ravichandran and the matching funds provided by the Dow Chemical Company for this research is gratefully

acknowledged. The authors would like to thank Drs Michael El-Raheb, William Rafaniello and Kwanho Yang of Dow Chemical Co., Midland, MI, for many useful discussions during this investigation.

References

1. L. M. SHEPPARD, *Ceram. Bull.* **69** (1990) 1801.
2. T. J. MROZ, *ibid.* **71** (1992) 1782.
3. H. C. HEARD and C. F. CLINE, *J. Mater. Sci.* **15** (1980) 1889.
4. W. CHEN and G. RAVICHANDRAN, *J. Amer. Ceram. Soc.* **77** (1994) 263.
5. J. C. GLANDUS, J. L. BESSON and P. BOCH, *Sci. Ceram.* **11** (1981) 419.
6. G. DE WITH and N. HATTU, *J. Mater. Sci.* **18** (1983) 503.
7. Z. C. JOU and A. V. VIRKAR, *J. Amer. Ceram. Soc.* **73** (1990) 1928.
8. Z. ROSENBERG, N. S. BRAR and S. J. BLESS, *J. Appl. Phys.* **70** (1991) 167.
9. S. R. WITEK, G. A. MILLER and M. P. HARMER, *J. Amer. Ceram. Soc.* **72** (1989) 469.
10. H. KOLSKY, *Proc. R. Soc. Lond.* **B62** (1949) 676.
11. S. NEMAT-NASSER, J. B. ISAACS and J. E. STARRETT, *ibid.* **A435** (1991) 371.
12. G. SUBHASH and S. NEMAT-NASSER, *J. Amer. Ceram. Soc.* **76** (1993) 153.
13. G. SUBHASH and S. NEMAT-NASSER, *J. Mater. Sci.* **28** (1993) 5949.
14. G. RAVICHANDRAN and G. SUBHASH, *J. Amer. Ceram. Soc.* **77** (1994) 263.
15. W. CHEN, G. SUBHASH and G. RAVICHANDRAN, *DYMAT J.* **1** (1992) 193.
16. I. O. OWATE and R. FREER, *J. Amer. Ceram. Soc.* **75** (1992) 1266.
17. J. LANKFORD, *ibid.* **64** (1981) C-33.
18. *Idem.*, *ibid.* **12** (1977) 791.
19. A. G. EVANS, *Int. J. Fract.* **10** (1972) 251.
20. D. E. GRADY and J. LIPKIN, *Geophys. Res. Lett.* **7** (1980) 255.
21. H. HORII and S. NEMAT-NASSER, *Phil. Trans. Roy. Soc. Lond.* **A319** (1986) 337.
22. M. F. ASHBY and S. D. HALLAM, *Acta Metall.* **34** (1986) 497.
23. L. B. FREUND, "Dynamic fracture mechanics" (Cambridge University Press, 1990).
24. G. RAVICHANDRAN and G. SUBHASH, *Int. J. Solids Structures* **32** (1995) 2627.
25. G. RAVICHANDRAN and R. J. CLIFTON, *Int. J. Fract.* **40** (1989) 157.
26. L. R. DEOBALD and A. S. KOBAYASHI, *J. Amer. Ceram. Soc.* **75** (1992) 2867.

Received 7 May 1996
and accepted 7 January 1997